CHAPTER 4

Measurement of $^{232}Th(n, \gamma)^{233}Th$ and $^{232}Th(n, 2n)^{231}Th$ reaction cross-sections using activation technique

4.1 Introduction 61

4.2 Six meter irradiation set-up at BARC-TIFR Accelerator Facility 64

4.2.1 Neutron Irradiation 66

4.3 Experimental Details 66

4.4 Analysis of Experimental Data 73

4.4.1 Calculation of the neutron energy 73

4.4.2 Calculation of the neutron flux 83

4.4.3 Determination of $^{232}Th(n, \gamma)^{233}Th$ and $^{232}Th(n, 2n)^{231}Th$ reaction cross-sections 85

4.5 Theoretical calculations of $^{232}Th(n, \gamma)^{233}Th$ and $^{232}Th(n, 2n)^{231}Th$ reaction cross-sections using nuclear model based computer code Talys 1.2 91

4.5.1 Nuclear Model based TALYS Code 91

4.5.2 Optical model potential 92

4.5.3 Pre-equilibrium reactions 93

4.5.4 Level densities 94

4.6 Result and Discussions 95

4.7 Summary and Conclusions 99

References 101

Published in:

1. **P. M. Prajapati** *et al.*, Measurement of the neutron capture cross-sections of ^{232}Th at 5.9 MeV and 15.5 MeV, Eur. Phys. J A **48**, 35 (2012)
2. H. Naik, **P. M. Prajapati** et al., Measurements of the neutron capture cross-sections of ^{232}Th using activation technique, Eur. Phys. J A **47**, 51 (2011)

4.1 Introduction

Accelerator driven sub-critical systems (ADS) [1-6] are of primary interest of recent times from the point of transmutation of long-lived fission products (^{93}Zr, ^{99}Tc, ^{107}Pd, ^{129}I and ^{135}Cs), and incineration of long-lived minor actinides (^{237}Np, ^{240}Pu, ^{241}Am, ^{243}Am and ^{244}Cm) to solve the problem of radioactive wastes. On the other hand, advanced heavy water reactor (AHWR) [7, 8] and fast reactors [9-12] are presently also of major interest. In AHWR, ^{232}Th-^{233}U is the primary fuel for power generation. However, ^{232}Th - ^{233}U fuel in connection with ADS is one of the possibilities for power generation besides transmutation of long-lived fission products and incineration of long-lived minor actinides. Besides these, thorium in the earth's crust is three to four times more abundant than uranium. Thus, it is a fact that ^{232}Th is the only nucleus present in nature which can give rise to an excess of fissile material ^{233}U in presence of either thermal or fast neutrons, and thus making it an excellent choice for nuclear reactors of the future.

In the ^{232}Th-^{233}U fuel cycle, the fissile nucleus ^{233}U is generated by two successive β-decays after a neutron capture by the fertile nucleus ^{232}Th. Further, the ^{232}Th(n,2n)^{231}Th reaction rapidly increases in importance for energies above threshold energy of 6.648 MeV. A schematic diagram of the Th-U fuel cycle is given below in Fig. 4.1.

$$\begin{array}{ccccccc}
 & & & \beta^- & & \beta^- & \\
^{232}\mathrm{Th}\,(n,\gamma) & \rightarrow & ^{233}\mathrm{Th} & \rightarrow & ^{233}\mathrm{Pa} & \rightarrow & ^{233}\mathrm{U} \\
1.405\times10^{10}\ \mathrm{y} & & 22.3\ \mathrm{m} & & 26.97\ \mathrm{d} & & 1.52\times10^{5}\ \mathrm{y} \\
\downarrow (n,2n) & \beta^- & & & & \beta^- & \downarrow (n,2n) \\
^{231}\mathrm{Th} & \rightarrow & ^{231}\mathrm{Pa}\,(n,\gamma) & \rightarrow & ^{232}\mathrm{Pa} & \rightarrow & ^{232}\mathrm{U} \\
25.32\ \mathrm{h} & & 32760\ \mathrm{y} & & 1.31\ \mathrm{d} & & 68.7\ \mathrm{y}
\end{array}$$

Fig. 4.1 A Schamatic diagram of Th-U fuel cycle

Thus, the production of fissile nucleus ^{233}U depends on the ^{232}Th(n,γ) ^{233}Th reaction cross-section, which is required with an accuracy of 1-2 % for predicting the dynamical behavior

of complex arrangements in fast reactors or ADS [13, 14] safely. In fusion-fission hybrid systems, a sensitivity study has shown that the production rate of ^{233}U can be predicted within 1 %, provided that the $^{232}Th(n,\gamma)^{233}Th$ cross-section between 3 keV and 3 MeV is known within 2 % [15]. In fast breeder reactors, the most important region for neutron capture of ^{232}Th lies between 10 keV to 100 keV [16]. However, in ADS the energy of neutrons is on higher side. Thus, the $^{232}Th(n,\gamma)$ reaction cross-section at higher neutron energy has a strong impact on the performance and safety assessment for ADS [17]. In ADS, a 10 % change in the ^{232}Th neutron capture cross-section gives rise to a 30 % change in the needed proton current of the accelerator if the system has to be operated at a sub-critical level of $K_{eff} \approx 0.97$ [18].

Therefore, there is a general interest in determining the neutron capture cross-section of ^{232}Th for energy applications involving the Th-U fuel cycle from the point of view of the nuclide inventory calculations. For India, which has abundant reserves of thorium, ADS based on the Th-U fuel cycle is relevant because one can exploit its potential to design hybrid reactor system that can produce nuclear power with the use of thorium as a main fuel [19]. The ^{232}Th - ^{233}U fuel cycle has an added advantage that it minimizes the production of the troublesome long lived actinide waste. The ADS based thorium burners may need only small and limited quantities of uranium and plutonium fuel to serve as starter seeds. When using thorium as a nuclear ADS fuel, the study of the production of problematic transthorium is essential.

The measurement of the neutron capture cross-sections for ^{232}Th above 2 MeV is challenging task due to low cross-section (< 50 mb) as well as the competition with other reaction channels (fission, inelastic) create major difficulties for methods based on γ-ray detection. Therefore, it is worthwhile to determine neutron capture cross-sections for ^{232}Th between 2 MeV and 14.5 MeV since few data exist [20]. A detailed literature survey shows that there are a lot of $^{232}Th(n,\gamma)$ reaction cross-section data over a wide range of neutron energies from thermal to 2.73 MeV based on physical measurements [21-23] and activation technique [24-36]. Beyond 2.73 MeV, only one data of the $^{232}Th(n,\gamma)$ reaction cross-section is available at 14.5 MeV [37] using the activation technique. From these data, it can be seen that the $^{232}Th(n,\gamma)$ reaction cross-section decreases monotonically from 20 eV to 2.73 MeV. There is no data in between 2.73 MeV and 14.5 MeV. The earlier measurement at neutron energy (E_n) of 14.5 MeV

[37] is not interpreted by model calculations as there are no data to tune essential parameters. Further, the ^{232}Th(n, 2n) reaction starts and becomes the pre-dominant mode beside fission and inelastic reaction channels above neutron energy of 6.4 MeV. There are lots of data on ^{232}Th(n,2n) reaction cross-section are available in the literature from physical measurement [38] and from off-line activation methods [39-46]. It can be seen from these data that the ^{232}Th (n, 2n) reaction cross-section increases from 6.44 MeV up to the neutron energy of 9.86 MeV and then remains constant up to 13-14 MeV. There after it decreases monotonically. Adjacent to neutron energy of 6.4 MeV, there is no ^{232}Th(n,γ) reaction cross-section data available to examine its trend, where the ^{232}Th(n,2n) reaction starts .

In view of the above explanation and discussion, the work mentioned in this chapter is carried out with the following objectives:

- Measurement of ^{232}Th(n, γ)^{233}Th reaction cross-section at average neutron energies (E_n) of 3.7 MeV, 5.9 MeV, 9.85 MeV and 15.5 MeV using activation and off-line γ-ray spectrometric technique.

- Measurement of ^{232}Th(n, 2n) ^{231}Th reaction cross-section at average neutron energies (E_n) of 9.85 MeV and 15.5 MeV using the same techniques as mentioned above.

- Comparison of experimentally measured data with latest available evaluated nuclear data libraries such as ENDF/B-VII.0 [47], JENDL 4.0 [48] and JEFF 3.1 [49].

- Reproduction of the experimental results using theoretical calculations by nuclear reaction model based computer code Talys 1.2 [50].

The experiments for the measurement of ^{232}Th(n, γ)^{233}Th and ^{232}Th(n, 2n) ^{231}Th reaction cross-sections have been carried out using the 14UD BARC-TIFR Pelletron facility at Mumbai, India. The neutron beam was generated using the ^{7}Li(p, n) reaction [51] from the proton beam main line at 6 m above the analyzing magnet of the Pelletron facility to utilize the maximum proton current from the accelerator.

4.2 Six meter irradiation set-up at BARC-TIFR Pelletron Facility

The Bhabha Atomic Research Centre – Tata Institute of Fundamental Research (BARC-TIFR) pelletron facility at TIFR, Mumbai has been a major centre for heavy ion [52] accelerator based research in India since its commissioning in 1989 .The Accelerator is housed inside a tank which is 6 meter in diameter and 25 meter long. A photograph of the 6 M irradiation set-up is shown in Fig. 4.2. The 6 M irradiation set-up is operational in the tower area and being utilized for many applications since 2003 [53]. The radiation shielding of the accelerator tower can accommodate beam currents of few μA but cannot be delivered to the Pelletron beam hall due to the inadequate radiation shielding there. The Layout of drift space above analyzing magnet has been modified to accommodate 6M irradiation setup in tower area itself. The proton beam of energy 2 MeV to 24 MeV up to μA current range can be taken on targets at this port. The accelerator complex and surrounding area are within the permissible radiation limit when high proton beam current is accelerated.

There are three gate valves in this setup. The lower gate valve (BLV-6C) remains close during the experiments. The upper gate valve (BLV-6A) isolates tank bottom beam line. The 6M experimental chamber is connected to a Turbo Molecular pump (500lit/sec) with an isolation valve (BLV-6B). The Pneumatically operated BLV-6A and BLV-6C is vacuum interlocked. The cold cathode gauge at 6M chamber senses vacuum and accordingly sends signal to an indigenously developed controller. This controller sends signal to coil of these valves to operate in case of power failure/accidental air rush, hence provides safety to accelerator.

The 6M experimental chamber can be isolated from accelerator by closing gate valves BLV 6A, 6B and 6C. Dry N_2 is inlet in chamber. Solid target is loaded on a stem which is water cooled and welded on a four inch NEC flange. This assembly is fixed on 6 M chamber. The beam current on targets can be measured by keeping another stem in forward direction, which works as faraday cup. After getting vacuum of $5x\ 10^{-7}$ torr with help of turbo pump, gate valve 6A is being opened. After securing area, accelerated beam from Pelletron enters in 6 M chamber and falls on target.

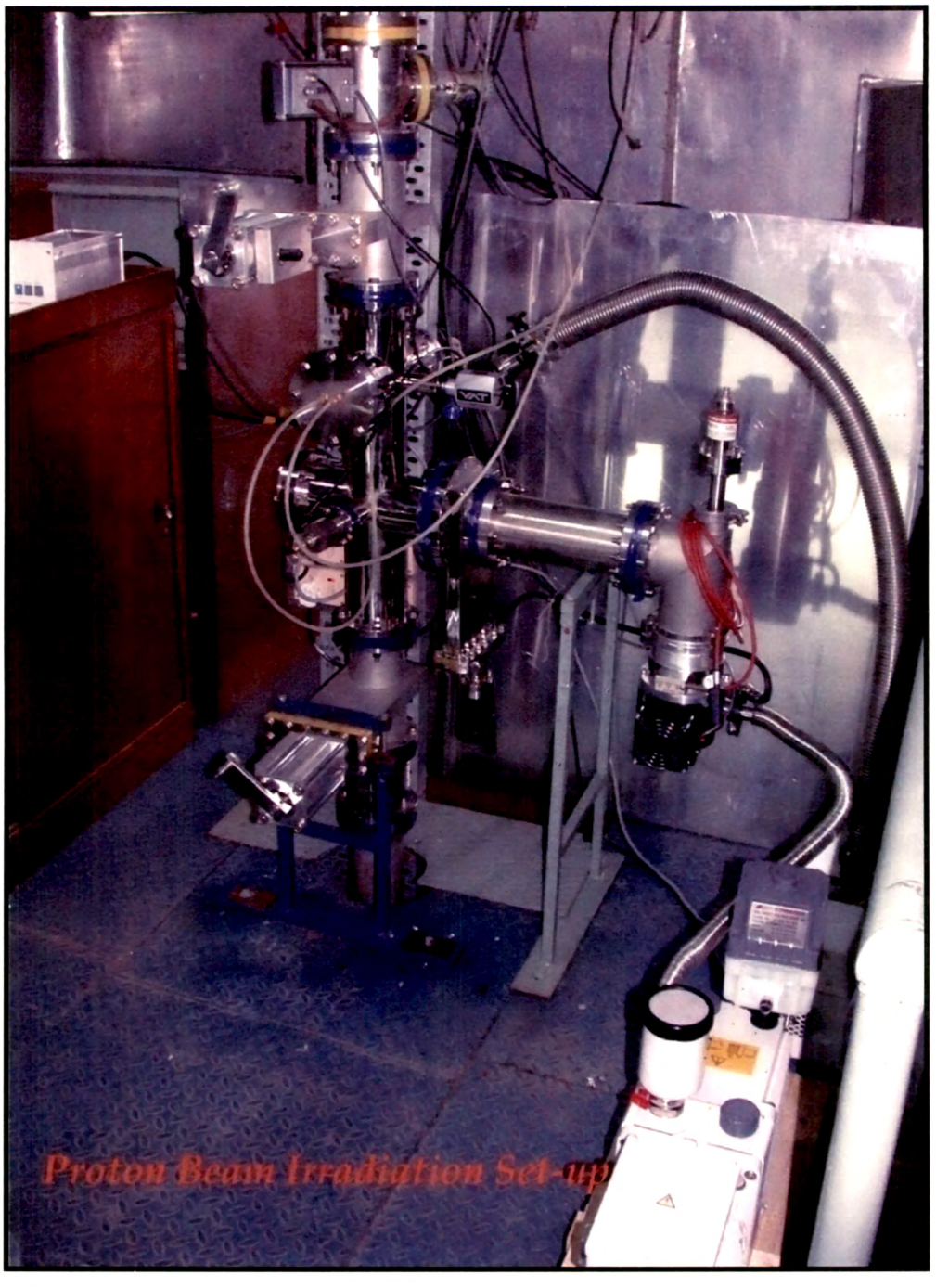

Fig. 4.2 Six meter Proton Beam Irradiation set-up at BARC-TIFR Pelletron, Mumbai

The target assembly, however, depending on activity level may not be replaced immediately, thereby affecting beam utilization. Moreover, in order to change the target dry Nitrogen is to be let in on each replacement. In order to resolve this problem, a multi target assembly has been designed, fabricated and being used at our facility.

The proton beam setup is being used to produce useful isotopes by Radio Chemistry Division and Radio Pharmaceutical Division, BARC. The same setup can be used to irradiate the target by an ion beam having different charge states (which means essentially different energies corresponding to the terminal voltage) at the same time.

4.2.1 Neutron Irradiation

As proton beam of energy 2 MeV to 24 MeV up to μA current range can be taken at 6 M irradiation setup. High energy neutrons can be produced via ^{7}Li(p, n) ^{7}Be* reaction. These neutrons are used to irradiate solid samples. This method has been used to measure neutron-induced reaction cross-sections for fertile materials (^{232}Th and ^{238}U) and various structural materials used in reactors which has an immense importance for the development of advanced reactors and Accelerator Driven Systems.

4.3 Experimental Details

The experiment was carried out using the 14 UD BARC-TIFR Pelletron Facility at Mumbai, India. The neutron beam was obtained from the ^{7}Li(p,n) reaction by using the proton beam main line at 6 meter above the analyzing magnet of the Pelletron Facility to utilize the maximum proton current from the accelerator. The energy spread for proton at 6 meter was maximum 50-90 keV. At this port, the terminal voltage is regulated by GVM mode using terminal potential stabilizer. Further, we use a collimator of 6 mm diameter before the target. The lithium foil for the first run was made up of natural lithium with thickness 3.7 mg/cm^2, sandwiched between two tantalum foils of different thickness. For the second run, the thickness of natural lithium foil was taken as 3.2 mg/cm^2 to minimize the energy loss. The front tantalum foil facing the proton beam was the thinnest one (3.9 mg/cm^2), in which degradation of proton energy, according to SRIM [54], was about 50-80 keV. On the other hand, the back tantalum foil was the thickest (0.025 mm), which was sufficient to stop the proton beam. Behind the Ta-Li-Ta

stack, the samples used for irradiation were natural ^{232}Th metal foil and natural indium metal foil, which were wrapped separately with 0.025 mm thick aluminum foil to prevent contamination from one to the other. The size of ^{232}Th metal foil was 1.0 cm^2 with thickness of 29.3 mg/cm^2, whereas indium metal foil is also of same size with thickness of 2.6 mg/cm^2. The γ-ray activity of ^{115m}In from ^{115}In(n,n')^{115m}In reaction was used to measure the neutron flux. The isotopic abundance of ^{115}In in natural indium is 95.7 %. The Th-In stack was mounted at zero degree with respect to the beam direction at a distance of 2.1 cm from the location of the Ta-Li-Ta stack. A schematic diagram of Ta-Li-Ta stack and Th-In stack is given in Fig.4.3. Different sets of stacks were made for different irradiations for various neutron energies.

The Ta-Li-Ta and Th-In stacks were irradiated for 12 h and 6 h depending upon the energy of proton beam facing the tantalum target. The energies of proton beam were 5.6 MeV and 12 MeV respectively during first experiment. Further, the Ta-Li-Ta and Th-In stacks were also irradiated at proton energies (E_p) of 7.8 MeV and 18 MeV for a period of 15 h and 5 h respectively during second experiment. The proton beam current during the irradiations was varied from 100 nA to 400 nA. After irradiation, the samples were cooled for one hour. Then, the irradiated target of Th and In along with Al wrapper were mounted in two different Perspex plates and taken for γ-ray spectrometry. The γ-rays of fission/reaction products from the irradiated Th and In samples were counted in an energy and efficiency calibrated 80 c.c. HPGe detector coupled to a PC-based 4K channel analyzer at Radiochemistry lab, TIFR, Mumbai as shown in Fig. 4.4. This detector set-up was purchased in a major DAE-BRNS project of Dr. S. Mukherjee.

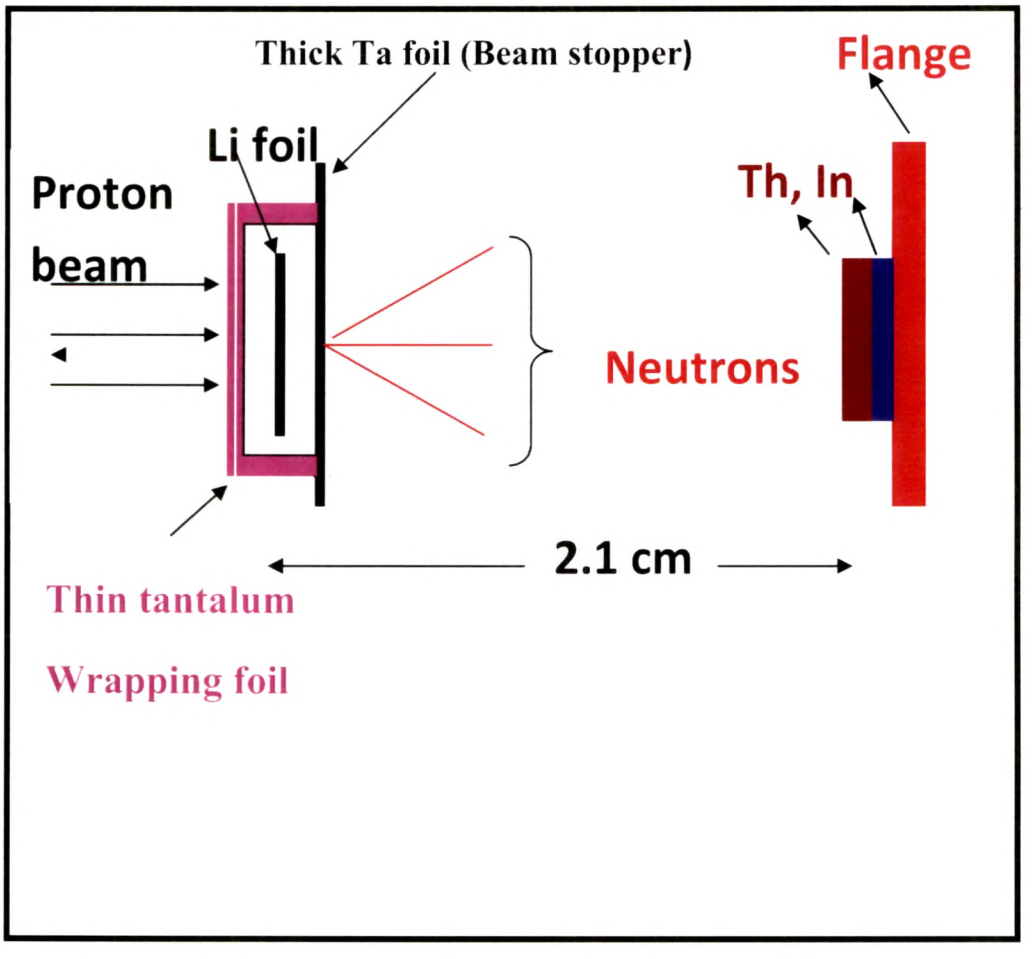

Fig. 4.3 A Schematic diagram showing the arrangement used for neutron irradiation

Fig. 4.4 High Purity Germanium (HPGe) Detector at RCD lab, TIFR, Mumbai

The counting dead time was kept always less than 5 % by placing the irradiated Th and In samples at a suitable distance from the detector to avoid pileup effects. The energy and efficiency calibration of the detector system was done by counting the γ-ray energies of standard ^{152}Eu and ^{133}Ba sources keeping the same geometry, where the summation error was negligible. This was checked by comparing the efficiency obtained from γ-ray counting of standards such as ^{241}Am (59.54 keV), ^{133}Ba (80.997, 276.4, 302.9, 356.02 & 383.82 keV), ^{137}Cs (661.66 keV), ^{54}Mn (834.55 keV), ^{60}Co (1173.23 & 1332.5 keV). The detector efficiency was 20 % at 1332.5 keV relative to 3" diameter x 3" length NaI(Tl) detector. The uncertainty in the efficiency was 2-3 %. The resolution of the detector system had a FWHM of 1.8 keV at 1332.5 keV of ^{60}Co. The γ-ray counting of the irradiated Th and In samples were done alternately in the first day at Radiochemistry Division (RCD) laboratory, TIFR, Mumbai, India. The HPGe detector set-up is shown in Fig.3. From second day onwards γ-ray counting of only Th sample was done up to few months to check the half-life of the nuclides of interest at RCD, BARC, Mumbai. Typical γ-ray spectrums of the irradiated ^{232}Th sample are given in Figs. 4.5 and 4.6 for cooling time of 167 h and 74 h respectively.

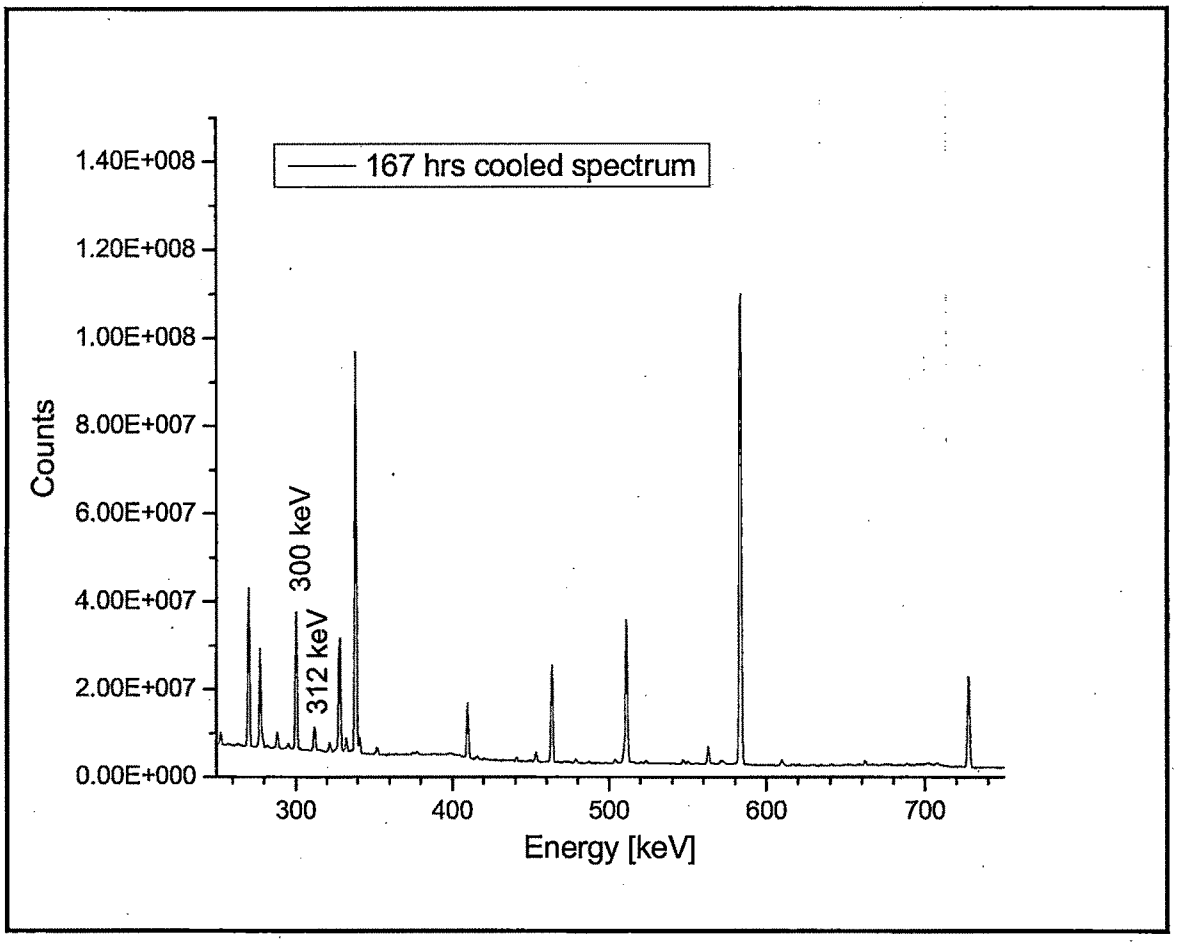

Fig. 4.5 Gamma ray spectrum of irradiated ^{232}Th showing the γ-ray energy of ^{233}Pa

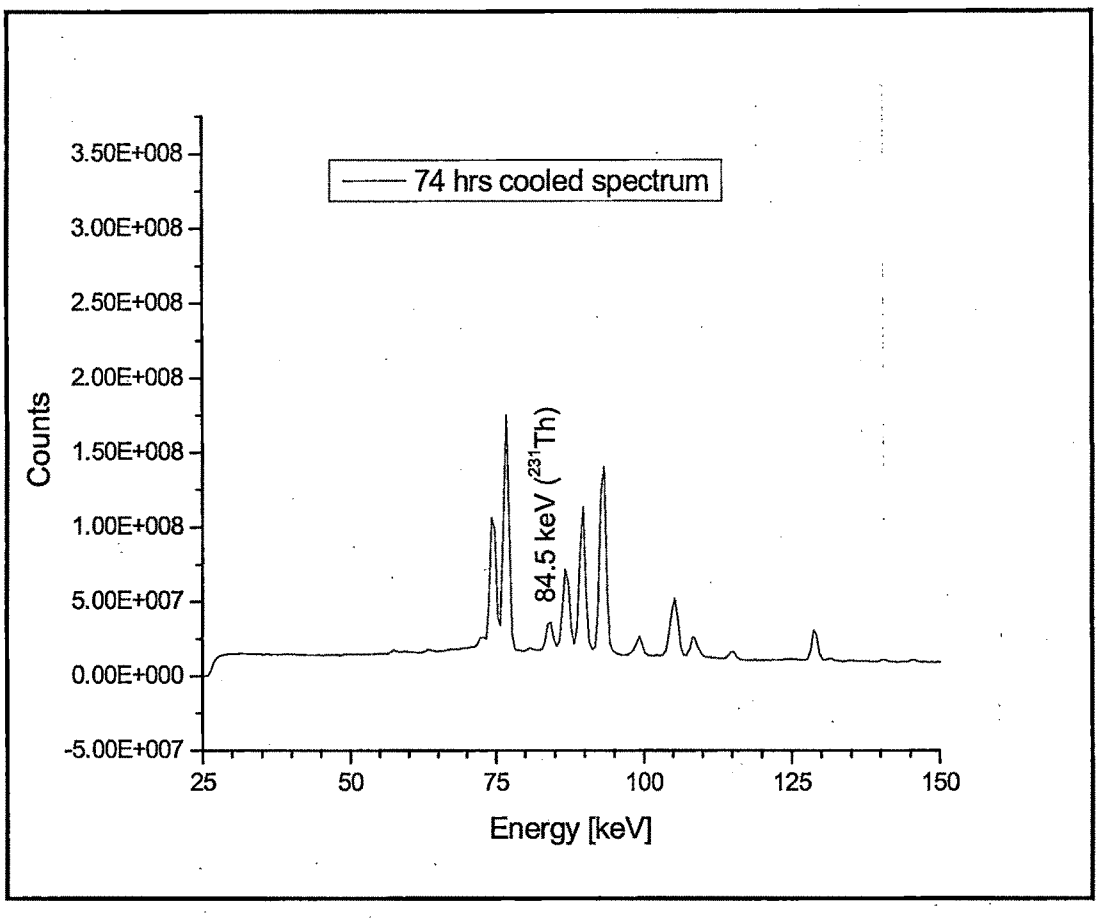

Fig. 4.6 Gamma ray spectrum of irradiated ^{232}Th showing the γ-ray energy of ^{231}Th

4.4 Analysis of Experimental Data

4.4.1 Calculation of the neutron energy

The $^{7}Li(p, n)^{7}Be$ reaction is used extensively as a source of fast neutrons. Below 2.38 MeV of proton energy, the reaction proceeds only to the ^{7}Be ground state and produces a single neutron group. At higher energies, other neutron-producing reactions can occur and they must be considered in the analysis of experimental results [55]. The usefulness of this neutron source at higher energies is severely limited by the presence of many neutrons from three-body break up reactions. The possibility of $^{7}Li(p, n)^{7}Be$ reaction as a neutron source at higher energies has been successfully explored for the first time by considering the presence of many neutrons from three-body break up reactions. The lithium targets have been used to be sufficiently thin so that only small fraction of the incident proton energy is dissipated in the lithium layer.

Natural lithium consists of the isotopes ^{6}Li and ^{7}Li with abundances 7.59 % and 92.41 % respectively [56]. The neutron-producing reactions to be considered for protons are given in Table 4.1. In practice, only the reactions labeled 3, 4 and 5 contribute to the number of neutrons, while reactions 1, 2 and 6 do not contribute significantly. Brochers and Poppe [57] found that the ratio of the yield from reaction 6 to that from reaction 3 is only about 2 % for $E_p = 9$ MeV and it is presumably smaller at lower energies. The low abundance of ^{6}Li and small cross-section would lead to small contributions for reactions 1 and 2. Brochers and Poppe, using natural-lithium targets, did not observe any neutrons from ^{6}Li [57].

Table 4.1 Different p + ^{6,7}Li reactions to produce energetic neutrons

Sr. No	Reaction	Q-Value (MeV)	Threshold energy (MeV)
1	^{6}Li(p, n)^{6}Be	-5.07	5.92
2	^{6}Li(p, np)^{5}Be	-5.67	6.62
3	**^{7}Li(p,n)^{7}Be (Ground state transition)**	**-1.644**	**1.88**
4	**^{7}Li(p, n)^{7}Be* *(First excited-state transition)**	**-2.079**	**2.38**
5	**^{7}Li(p, n^{3}He)^{4}He (Three-body break up reaction)**	**-3.23**	**3.68**
6	^{7}Li(p, n)^{7}Be** **(Second excited-state transition)**	-6.18	7.06

In the present experiments, the incident proton energies were 5.6 MeV, 7.8 MeV, 12 MeV and 18.0 MeV. The degradation of the proton energy in the front thin tantalum foil was only 50-80 keV. The Q-value for the ^{7}Li(p, n)^{7}Be reaction to the ground state is -1.644 MeV whereas the first excited state is at 0.431 MeV above the ground state leading to the Q-value -2.079 MeV. Therefore, for the proton energies of 5.6 MeV, 7.8 MeV, 12 MeV and 18.0 MeV, the resulting peak energies for the first group of neutrons (n_0) are3.96 MeV, 5.92 MeV, 10.36 MeV and 16.12 MeV respectively. The corresponding neutron energy of the second group neutrons (n_1), for the first excited state of ^{7}Be are 3.53 MeV, 5.42 MeV, 9.87 MeV and 15.62 MeV for the proton energies of 5.6 MeV, 7.8 MeV, 12 MeV and 18.0 MeV, respectively. This is because above proton energy of 2.4 MeV, the n_1 group of neutrons is also produced. H. Liskien and A. Paulsen [58] have given the branching ratio to the ground state and first excited state of ^{7}Be up to proton energy of 7 MeV. Based on their prescription for the proton energy of 5.6 MeV, the contribution to n_0 and n_1 group of neutrons are 86.1% and 13.9% respectively. The proton energy of 5.6 MeV leads to average neutron energy of 3.72x0.861+3.23x0.139 = 3.651 MeV. However, there is no data of the branching to first excited state at proton energy above 7 MeV. In view of this, the neutron spectrum at proton energy of 5.6 and 12 MeV were calculated using computer code EMPIRE-II [59]. Typical neutron spectrums from EMPIRE-II computer code are shown in Fig. 4.7 and 4.8.

From Fig. 4.7 and 4.8, it can be seen that the neutron spectrum is continuous with peaking at 3.3 MeV and 8.7 MeV for proton energy of 5.6 MeV and 12 MeV, respectively. Above incident proton energy of 3.7 MeV, the break up channel (^{8}Be$\rightarrow$n+^{3}He+^{4}He) also contributes. Therefore, owing to three body energy distribution, the neutrons spectrum should not be continuous but have tailing part in the lower energy region. These neutrons from breakup should have maximum of $E_{c.m}$ - 3.7 MeV only, which has not been found in the EMPIRE output. According to Prof. Roberto CapoteNoy, Nuclear Data Section, International Atomic Energy Agency (I.A.E.A), EMPIRE does not calculate properly reactions on light nuclides (to apply it below Al-27 is risky). There are compelling physical reasons for this as too few nucleons means that the statistical hypothesis does not hold. Moreover light nuclides need a proper account of direct transfer reactions that are not accounted for, or are considered in a very approximate way

in EMPIRE (break-up, pick-up, etc). Having said that is clear that one cannot get p+ ^{7}Li spectra out of EMPIRE calculations

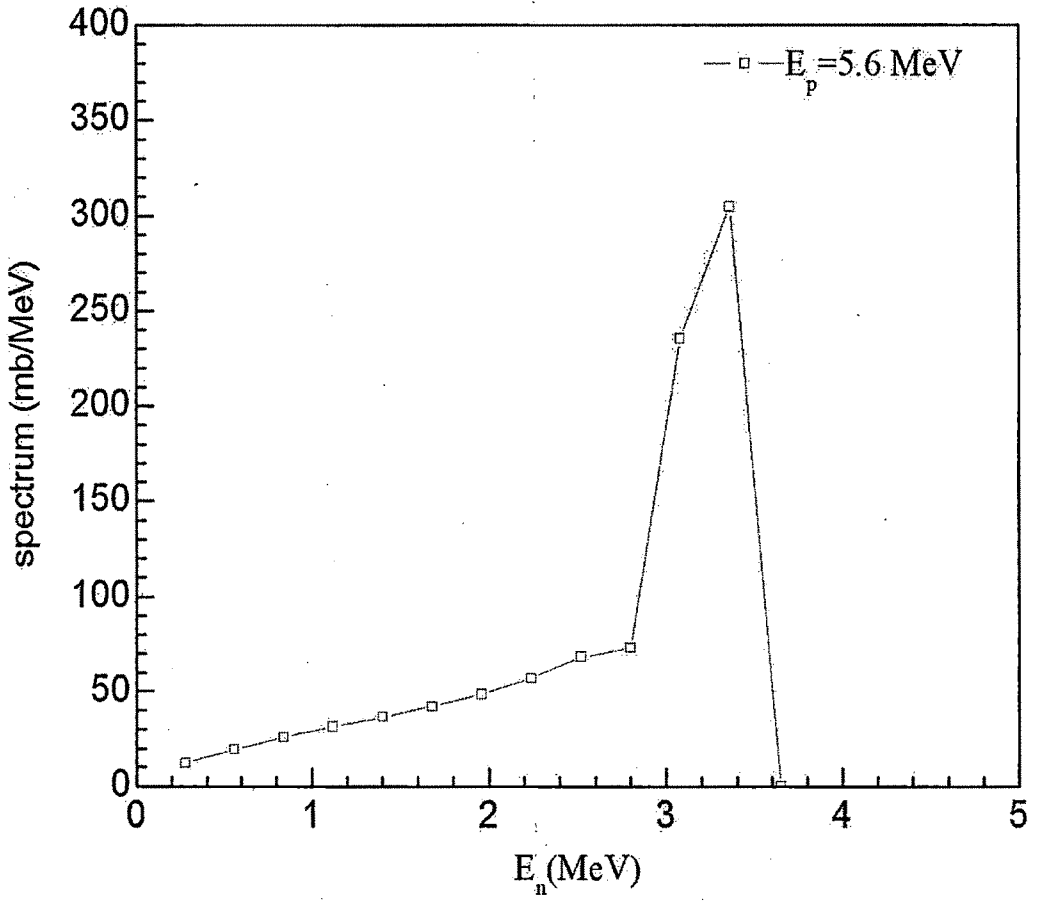

Fig. 4.7 Neutron spectrum from ^{7}Li(p,n) reaction irradiated with proton energy of 5.6 MeV calculated using EMPIRE computer code.

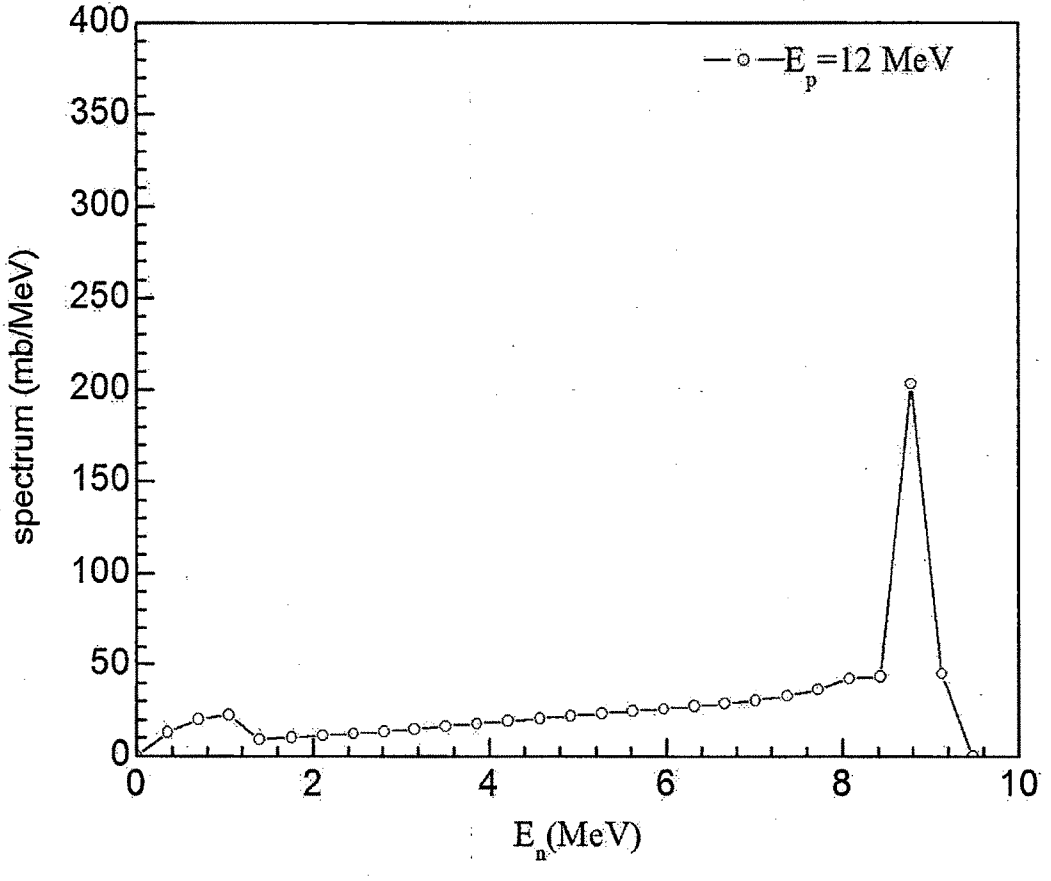

Fig. 4.8 Neutron spectrum from ^{7}Li(p,n) reaction irradiated with proton energy of 12 MeV calculated using EMPIRE computer code.

However, C.H. Poppe et al. [60] have given the branching ratio to ground state and first excited state of ^{7}Be for the proton energy of 4.2 MeV to 26 MeV. In addition to these, J. W. Meadows and D.L. Smith [55] have also given the branching ratio to the ground state and first excited state ^{7}Be up to 7 MeV. Based on their prescription for the proton energy of 5.6 MeV, the proton energy of 5.6 MeV leads to average neutron energy of 3.72x0.861+3.23x0.139 = 3.651 MeV. For proton energy of 12 MeV, the contributions to n_0 and n_1 group of neutrons are 60% and 40% respectively [60]. This leads to average neutron energy of 9.924 MeV.

Further, the fragmentation of ^{8}Be to ^{4}He + ^{3}He + n (Q = -3.23 MeV) occurs and other reaction channel opens to give a continuous neutron energy distribution besides n_0 and n_1 groups of neutrons above E_p = 4.5 MeV. J. W. Meadows and D.L. Smith have given experimental neutron distributions from break-up channels and also parameterized these distributions. For the proton energy of 5.6 MeV, the author has used their parameterization for break up neutrons having a weight of 4% and two Gaussian distributions with weights of 84% and 12% for n_0 and n_1 groups of neutron, which is shown in Fig. 4.9. These Gaussians are centered at 3.7 MeV and 3.2 MeV having a width of 0.3 MeV. For proton energy of 12 MeV, the author has extrapolated from the experimental neutron spectrum of C.H. Poppe et al. [60] to obtain the neutron spectrum, which is shown in Fig. 4.10. The average neutron energy for (n,γ) and (n,2n) reactions was obtained as 9.85±0.38 MeV after removing the tailing distribution of the neutron spectrum below 6.5 MeV from Fig.10. This value is slightly lower than the value of 9.924 MeV, which was calculated based on percentage weights of the two groups as mentioned above.

Similarly, the neutron energies for the incident proton energies of 7.8 MeV and 18 MeV have also been calculated. To observe the trend of a continuous neutron spectrum besides from n_0 and n_1 groups of neutrons for the proton energies of 7.8 MeV and 18.0 MeV, the neutron spectrum have been generated using the neutron energy distribution given by C. H. Poppe et al which are given in Figs. 11 and 12. The average neutron energies under the main peak region (n_0 and n_1 groups) have been calculated as 5.9±0.6 MeV and 15.5±0.7 MeV after removing the tail region for the proton energies of 7.8 MeV and 18.0 MeV, respectively from Figs. 4.11 and 4.12.

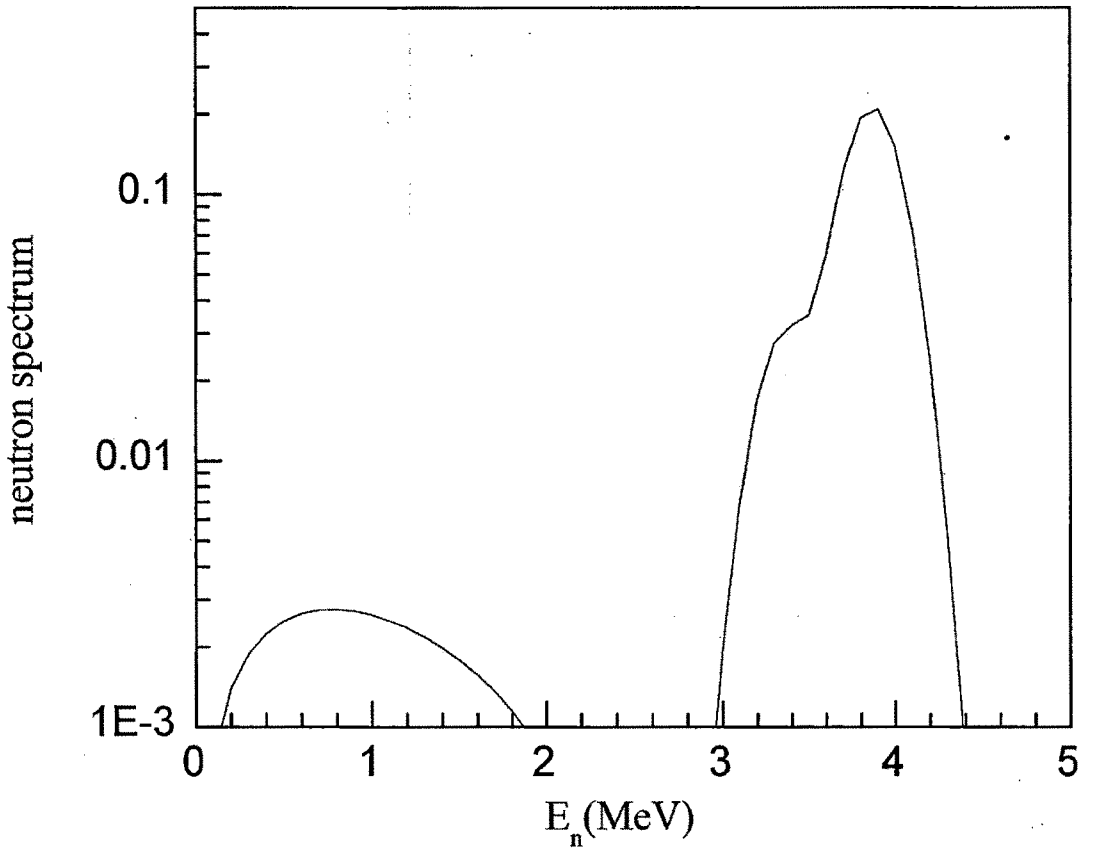

Fig. 4.9 Neutron spectrum from ^{7}Li(p,n) reaction at E_p=5.6 MeV calculated using the results of Meadows and Smith [55].

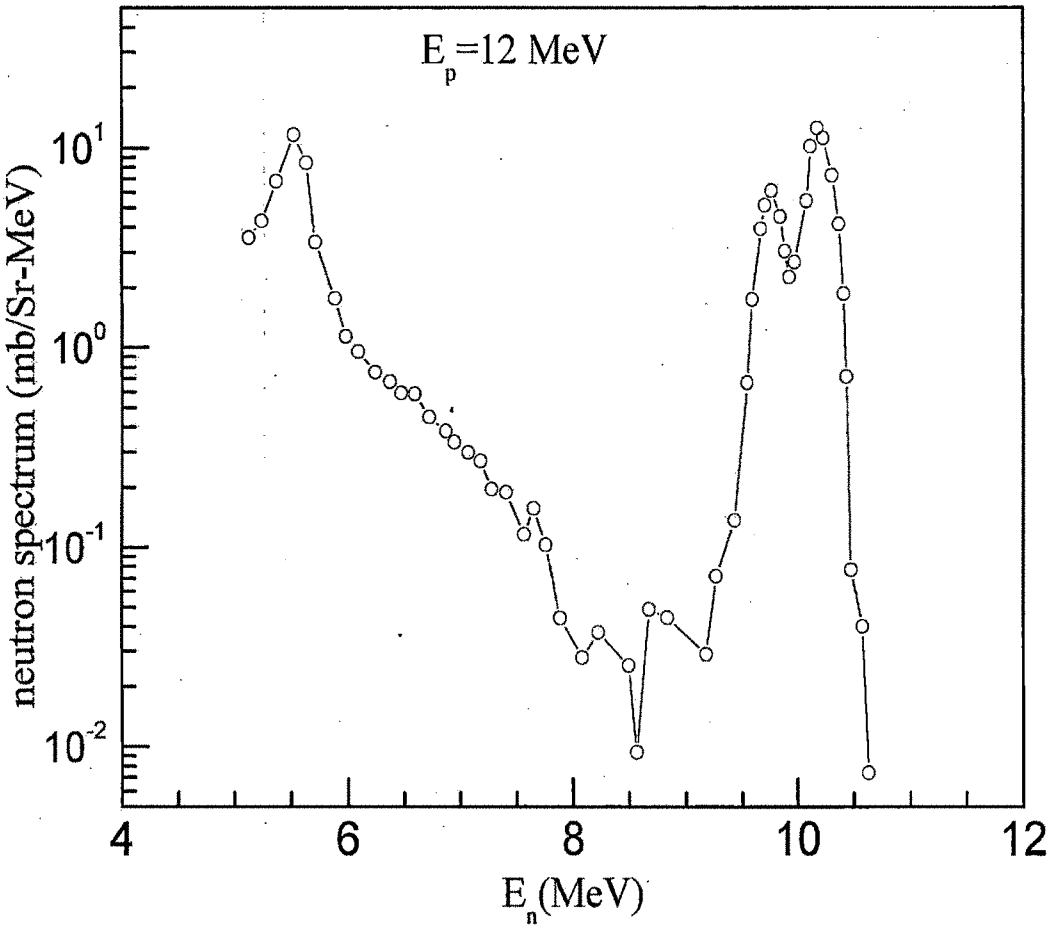

Fig. 4.10 Extrapolated neutron spectrum in ^{7}Li(p,n) reaction at E_p=12 MeV obtained from neutron spectrum at E_p=10 MeV of C. H. Poppe et al. [60]

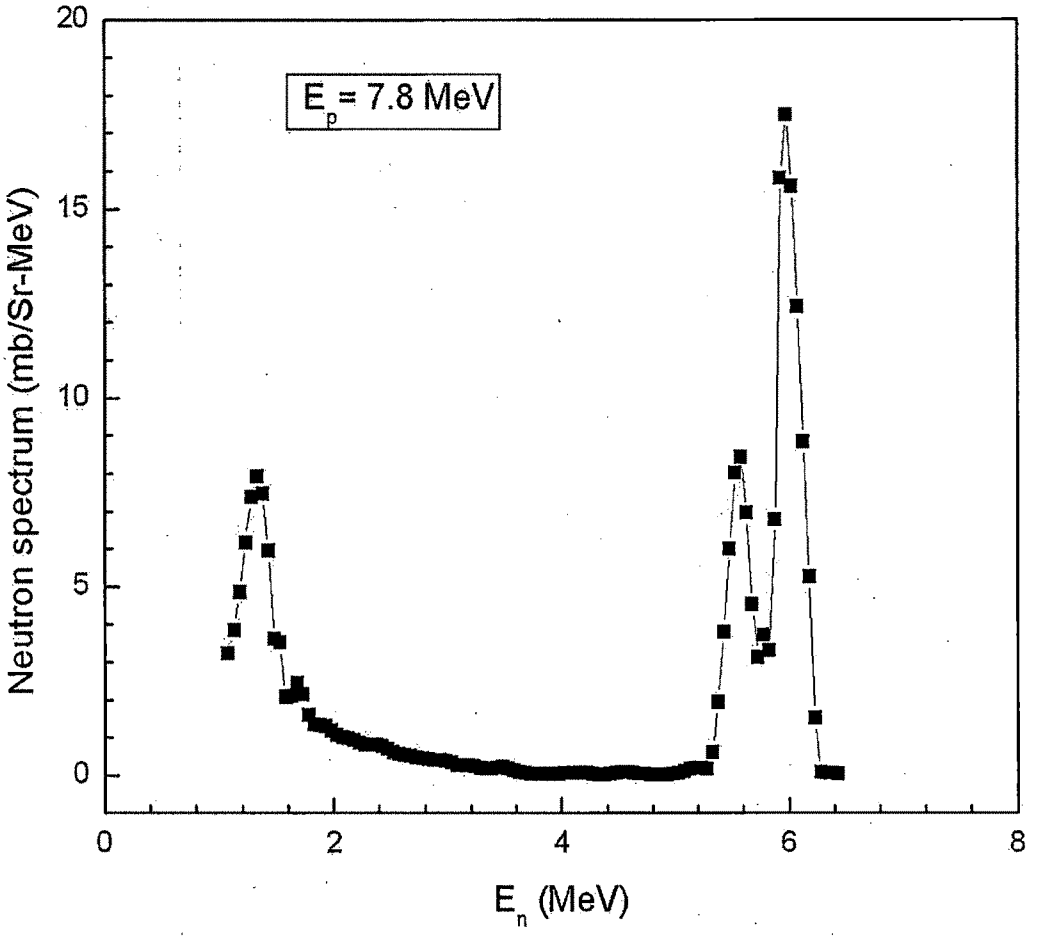

Fig. 4.11 Neutron spectrum from ^{7}Li(p, n) reaction at E_p=7.8 MeV calculated using the results of C. H. Poppe et al. [60]

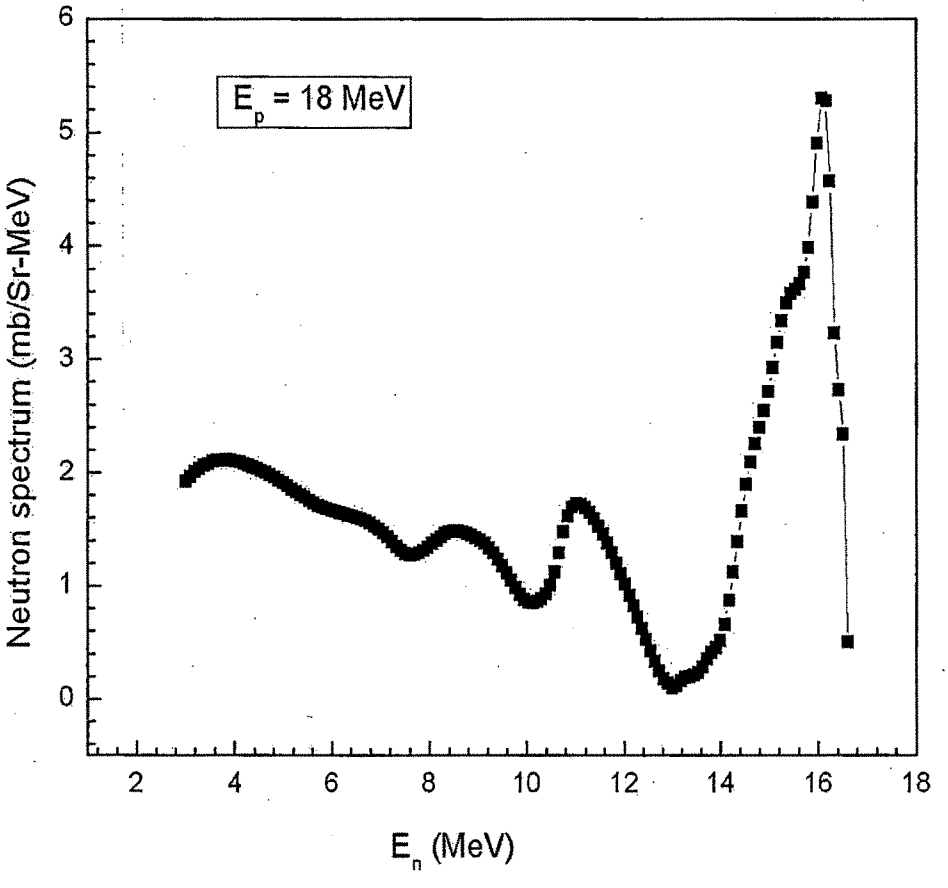

Fig. 4.12 Neutron spectrum from ^{7}Li(p, n) reaction at E_p=18 MeV calculated using the results of C. H. Poppe et al. [60]

4.4.2 Calculation of the neutron flux

In mono-energetic nuclear reactions, the neutron flux is usually obtained by using $^{197}Au(n,\gamma)^{198}Au$ and $^{115}In(n, n')^{115m}In$ reaction cross-sections. At low energy and for thermal neutrons, the photo-peak activity of 411.8 keV γ-line of ^{198}Au from $^{197}Au(n,\gamma)$ reaction is used for flux determination. At higher energy, the photo-peak activity of 336.2 keV γ-line of ^{115m}In from $^{115}In(n, n')$ reaction is used for flux determination. In the present work since the neutron energy from $^{7}Li(p,n)^{7}Be$ reaction is on the higher side, the $^{115}In(n, n')^{115m}In$ reaction has been used for neutron flux determination at proton energy of 5.6 MeV. The observed photo-peak activity (A_{obs}) for 336.2 keV gamma lines of ^{115m}In is related to the neutron flux (Φ) with the following relation,

$$Aobs\left(\frac{CL}{LT}\right) = N\sigma\varphi\alpha\varepsilon\,(1 - e(-\lambda t)e(-\lambda T)(1 - e(\lambda CL)/\lambda \quad (1)$$

where,

N = number of target atoms

σ = monitor reaction cross-section

α = branching intensity γ-lines

ε = branching detection efficiency

t = irradiation time

T = cooling time

CL = clock time

LT = counting time

In the above equation the CL/LT term has been used for dead time correction.

The observed photo-peak activity (A_{obs}) of 336.2 keV γ-lines of ^{115m}In was obtained using PHAST peak fitting program [61]. The σ values for $^{115}In(n, n')^{115m}In$ reaction were taken from

ref. [62] for the determination of neutron flux. The nuclear spectroscopic data such as half-life and branching intensity (a) were taken from refs. [63]. The neuron flux (Φ) at the neutron energy of 3.7 MeV was obtained to be 1.6 x10^6 n cm^{-2} s^{-1}. In the ^{7}Li(p, n)^{7}Be reaction, there is a contribution of 13.9 % from second group at neutron energy of 3.23 MeV. Thus the σ values of 13.9 % contribution at 3.23 MeV and 86.1 % at 3.72 MeV were considered for the determination of neutron flux. In order to examine this, the neutron flux was also calculated using the yield (Y) of fission products as ^{92}Sr or ^{97}Zr, extracted from the experimental yields of ref. [64] in the 3.7 MeV neutron induced fission of ^{232}Th. The following equation was used for such calculation.

$$\varphi = \frac{Aobs\left(\frac{CL}{LT}\right)\lambda}{N\sigma fYas(1-\exp(-\lambda t))\exp(-\lambda T)(1-\exp(\lambda CL))} \qquad (3)$$

All terms in Eq. (2) have the same meaning as in Eq. (1) except the yield (Y) of the fission product [64] and fission cross-section (σf), which was taken from ref. [65].

At average neutron energy of 3.7 MeV, the neutron flux calculated using Eq. (2) is 1.64 x10^6 n cm^{-2} s^{-1}, which is in close agreement with the value 1.6 x 10^6 n cm^{-2} s^{-1} obtained from Eq. (1). Further, folding the neutron spectrum of Fig. 8 with Th (n,f) cross section [65] at different neutron energies gives average fission cross-section. Using the average Th (n, f) cross section also gives the value of similar neutron flux. This is due to the negligible tailing in the neutron spectrum for E_n=3.7 MeV corresponding to the proton energy of 5.6 MeV (Fig. 4.9).

In the present work since the neutron energies are on higher side, the contribution from the second group and tailing due to break up (^{8}Be → ^{4}He + ^{3}He + n) is more important. It can be seen from Figs. 4.10, 4.11 and 4.12 that the tail regions of the low energy neutrons are quite significant. Within this range of neutron energy, the ^{115}In(n,n')^{115m}In reaction cross-section changes drastically [62]. On the other hand, the neutron-induced fission cross-section of ^{232}Th [65] also changes when increasing of neutron energy but the yield of fission products [64] at peak position of the mass-yield curve do not change significantly. In view of this, for the neutron energies of 5.9±0.6 MeV, 9.85±0.38 MeV and 15.5±0.7 MeV, neutron fluxes were calculated

using the yield of fission products (^{92}Sr, ^{97}Zr and ^{135}I) extracted from the experimental yields of refs. [64, 66] in the neutron induced fission of ^{232}Th. Using the Eq. (2), neutron fluxes were calculated as (3.53±0.21) x 10^6 n.cm^{-2}.sec^{-1}, (1.3 x10^7) n cm^{-2} s^{-1} and (1.54±0.08) x 10^7 n.cm^{-2}.sec^{-1} for the neutron energies of 5.9±0.6 MeV, 9.85±0.38 MeV and 15.5±0.7 MeV, respectively for the ^{232}Th(n, γ) reaction cross-sections calculation. The neutron fluxes for (n,2n) reaction at average neutron energy of 9.85±0.38 MeV and 15.5±0.7 MeV were obtained as (6.5 x10^6) n cm^{-2} s^{-1} and (1.05±0.08) x 10^7 n.cm^{-2}.sec^{-1} respectively. These values were obtained based on the ratio of neutron fluxes of the neutron spectrum of Figs. 4.10 and 4.12 for (n, 2n) reactions above its threshold to total flux.

4.4.3 Determination of ^{232}Th(n, γ)^{233}Th and ^{232}Th(n, 2n)^{231}Th reaction cross-sections

The nuclear spectroscopic data used in the present work for the calculation of ^{232}Th(n, γ) and ^{232}Th(n, 2n) reaction cross-sections were taken from the refs. [67, 68] and are given in Table 4.2. The half-life of ^{233}Th is 21.83 min., which decays 99.61% to ^{233}Pa within 3 h. Thus, the ^{232}Th (n, γ) cross-section was calculated from the observed photo-peak activity of ^{233}Pa ($T_{1/2}$ = 26.975 days) of long cooled spectrum. However, it can be seen from Table 2 that, for ^{233}Pa, the abundance of the 300.1 keV γ-ray is lower than the 311.9 keV. On the other hand, Fig. 5 shows that the peak area of 300.1 keV γ-line is higher than 311.9 keV γ-line. This is because of the interference with γ-line of the ^{212}Pb decay product from ^{232}Th, which can be seen from Fig. 4.13 from separated peak of ^{233}Pa. In view of this, the ^{232}Th(n γ) cross-section (σ) was calculated from the observed activity of 311.9 keV of ^{233}Pa in the γ-ray spectrum of the un-separated sample.

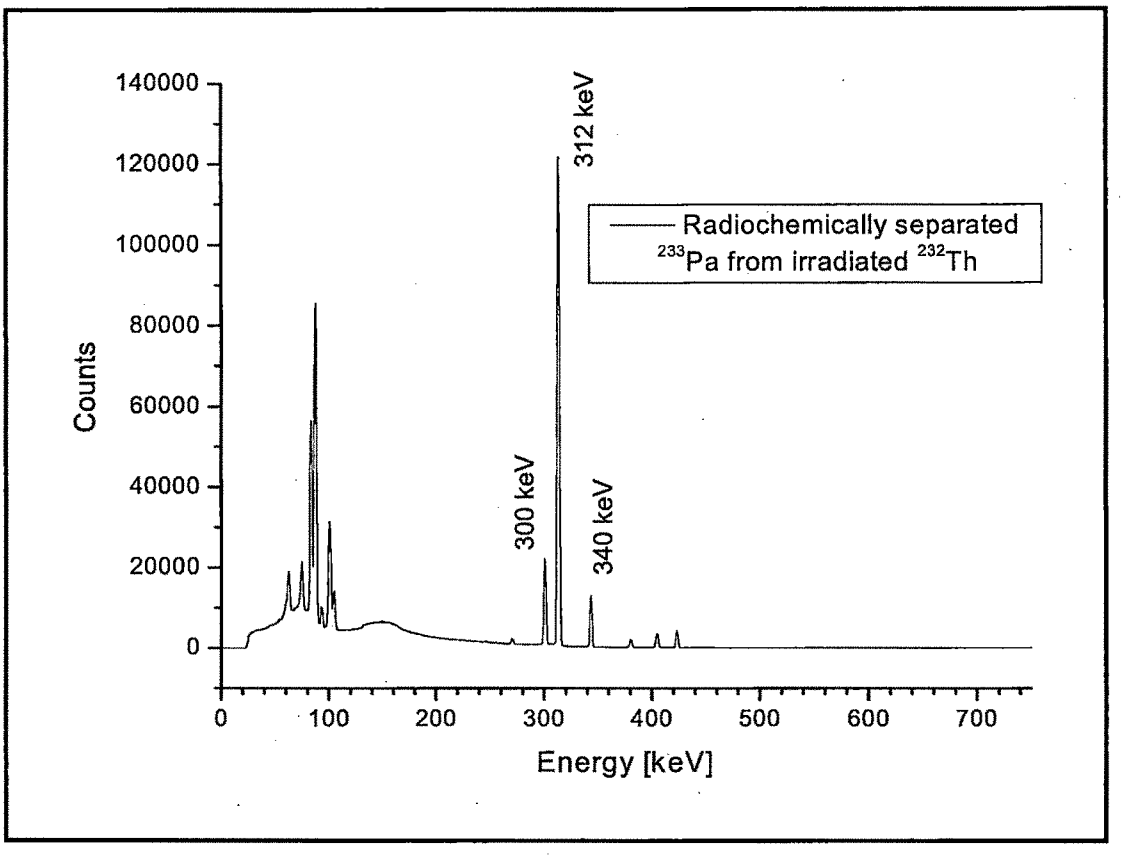

Fig. 4.13 Gamma ray spectrum of separated ^{233}Pa from neutron irradiated ^{232}Th

Table 4.2 Nuclear spectroscopic data used in the calculation

Nuclide	Half life	γ-ray energy (keV)	γ - ray abundance (%)
^{115m}In	4.486 h	336.2	45.9
^{231}Th	25.52 h	84.2	6.6
^{233}Th	21.83 m	86.5	2.7
^{233}Pa	26.975 d	300.1	6.63
		311.9	38..4
		340.8	4.47

Similarly, the ^{232}Th(n, 2n) reaction cross-section was also calculated from the observed photo-peak activity of 84.2 keV γ-line of ^{231}Th from the γ-ray spectrum after sufficient cooled spectrum. This is because the 84.2 keV γ-line of ^{231}Th in the γ-ray spectrum recorded within 3-4 hours interferes with the 86.5 keV of ^{233}Th having half-life of 21.83 minutes. The observed photo-peak activities (A_{obs}) of 84.2 keV γ-line of ^{231}Th and 311.9 keV γ-line of ^{233}Pa are obtained by using PHAST fitting program. The following equation was used for the calculation of the ^{232}Th(n, γ) and ^{232}Th(n, 2n) reaction cross-section (σ) as

$$\sigma = \frac{Aobs\left(\frac{CL}{LT}\right)\lambda}{N\varphi a\varepsilon\,(1-e(-\lambda t)e(-\lambda T)(1-e(\lambda CL)} \qquad (3)$$

All terms in Eq. (3) have the similar meaning as in the Eq. (1). We have calculated an uncorrected ^{232}Th(n, γ) reaction cross-section as 16.180±0.871 mb, 6.47±0.11 mb, 2.187±0.123 mb and 2.35±0.12 mb for the neutron energy spectrum generated from incoming proton energies of 5.6 MeV, 7.8 MeV, 12 MeV and 18 MeV, respectively. Furthermore, an uncorrected ^{232}Th(n, 2n) cross-section has also been calculated as 1722 ± 76 mb and 1680 ± 103 mb in the same way for the neutron energy spectrum generated from incoming proton energy of 12 MeV and 18 MeV, respectively.

From the Figs. 4.9, 4.10, 4.11 and 4.12, it is clear that low energy neutrons also contribute to the ^{232}Th(n, γ) cross-section. In view of this, the contributions from the tail region to ^{232}Th(n, γ) reaction have been estimated using the ENDF/B-VII.0, JENDL-4.0 and JEFF-3.1 libraries by folding the cross-section with neutron flux distributions of Figs. 4.9, 4.10, 4.11 and 4.12. The contributions to the ^{232}Th(n,γ) reaction from the above evaluations at E_P = 5.6 MeV are 5.34, 5.57 and 5.03 mb from ENDF/B-VII.0, JENDL-4.0 and JEFF-3.1 respectively. Further, the contributions to the ^{232}Th(n, γ) reaction are 5.32, 5.69 and 5.06 mb from ENDF/B-VII.0, JENDL-4.0 and JEFF-3.1 respectively at E_P = 7.8 MeV. Similarly at E_P = 12.0 MeV, contributions to the ^{232}Th(n, γ) reaction are 0.798 mb and 0.876 mb from ENDF/B-VII.0 and JENDL-4.0 respectively and for E_P = 18.0 MeV, contributions are 1.502 mb and 1.639 mb from

ENDF/B-VII.0 and JENDL-4.0 respectively. For these energies, JEFF-3.1 has not been used due to unavailability of evaluated data above 6.0 MeV. The actual value of ^{232}Th(n, γ) reaction-cross section under the main peak regions of the n_0 and n_1 groups of the neutron spectrum has been obtained after subtracting the average cross-section from the evaluations mentioned above by considering standard deviation from their arithmetic mean due to neutrons from tail region from the experimentally determined data. Thus, the actual experimentally obtained ^{232}Th(n, γ) reaction cross-sections at average neutron energies of 3.7±0.3 MeV, 5.9±0.6 MeV, 9.85±0.38 MeV and 15.5±0.7 MeV are 10.86 ± 0.87,1.13±0.21, 1.35 ± 0.12 and 0.78±0.18 mb, which are given in Table 4.3 along with correction values derived from different evaluations (ENDF/B-VII, JENDL-4.0 and JEFF-3.1) and with uncorrected experimentally determined values. The ^{232}Th(n,2n) reaction cross-section at average neutron energy of 9.85±0.38 MeV corresponding to proton energy of 12 MeV from present work is 1721.71 ± 75.61 mb, which is also given in the Table 3. The tail contribution for ^{232}Th(n, 2n) reaction is negligible at E_p= 12.0 MeV. Further, it is observed from the Fig. 12 that the ^{232}Th(n, 2n) cross-section tops in the tail region as shown in Fig. 15 (from 6. 6 to 13 MeV). Therefore, the contribution from the tail region to ^{232}Th(n, 2n) reaction has also been estimated using the ENDF/B-VII.0, JENDL-4.0 and JEFF-3.1 libraries are 747.24 mb, 747.60 mb and 745.84 mb respectively as mentioned above at E_P = 18.0 MeV. The corrected ^{232}Th(n, 2n) reaction cross-section is obtained after subtracting the average evaluated cross-section (e. g ENDF/B-VII.0, JENDL-4.0 and JEFF-3.1) from experimental data. Thus, the actual experimentally obtained ^{232}Th(n, 2n) reaction cross-section at average neutron energy of 15.5±0.7 MeV is 932.81±108.9, which is also given in Table 4.3.

Table 4.3 ^{232}Th(n,γ)^{233}Th and ^{232}Th (n,2n)^{231}Th reaction cross-sections at different neutron energies

Neutron Energy (MeV)	Neutron flux ($n.cm^{-2}s^{-1}$)	Cross-section (mb)		
		Uncorrected Expt.	Correction values (ENDF-B/VII, JENDL 4.0 and JEFF 3.1)	Corrected values
^{232}Th(n,γ)^{233}Th				
3.7±0.3	(1.6±0.04) x 10^6	16.18±0.87	5.32±0.75	10.86 ± 0.87
5.9±0.6	(3.53±0.21)x 10^6	6.47±0.11	5.36±0.18	1.13± 0.21
9.85±0.38	(1.3±0.05) x 10^7	2.18±0.12	0.83±0.09	1.35 ± 0.12
15.5±0.7	(1.54±0.08)x 10^7	2.35±0.12	1.57±0.14	0.78 ± 0.18
^{232}Th (n,2n)^{231}Th				
9.85±0.38	(6.5±0.25) x 10^6	1722 ± 76	----	1722 ± 76
15.5±0.7	(1.05±0.08)x 10^7	1680 ± 103	747± 3	933 ± 109

The uncertainties associated to the measured cross-sections come from the combination of two experimental data sets. This overall uncertainty is the quadratic sum of both statistical and systematic errors. The random error in the observed activity is primarily due to counting statistics, which is estimated to be 5-10 %. This can be determined by accumulating the data for an optimum time period that depends on the half-life of nuclides of interest. The systematic errors are due to uncertainties in neutron flux estimation (~6 %), the irradiation time (~2%), the detection efficiency calibration (~3 %), the half-life of the fission products and the γ-ray abundances (~2%). Thus the total systematic error is about ~6%. The overall uncertainty is found to range between 8 and 12%, coming from the combination of a statistical error of 5-10% and a systematic error of 6%.

4.5 Theoretical calculations of ^{232}Th(n, γ)^{233}Th and ^{232}Th(n, 2n)^{231}Th reaction cross-sections using nuclear model based computer code Talys 1.2

In order to improve the database by experimental measurements, model based calculations offer cost effective and broader applicability. These new calculations could allow to solve the discrepancies exist among the literature data. Precise measurement of neutron induced reactions in high energy domain serve the purpose of testing and recommending the input parameters required in model-based evaluations of cross-sections at high energies which are essential to support new nuclear energy systems. The TALYS code has opened up options for calculating cross sections for various nuclear reaction channels including complex particle emission. All optical model calculations are performed by ECIS-03 [69], which is a part of TALYS itself. In this model, the optical model potentials for local and global parameterization are given by Koning and Delaroche [70].

4.5.1 Nuclear Model based TALYS Code

The new version of model code TALYS is used to calculate the cross sections in the present investigated process. TALYS is a computer code system for the prediction and analysis of nuclear reactions. This code simulates reactions that involve neutrons, photons, protons, deuterons, tritons, hellions and alpha particles, in the energy range from 1 KeV to 200 MeV and for target nuclides $A \geq 12$. To achieve this, different nuclear reaction models are incorporated into a single code system. The calculations are based on a theoretical analysis that utilizes the

optical model, compound nucleus statistical theory and pre-equilibrium processes. The theoretical calculations have been performed within the frame work of Hauser-Feshbach statistical model theory [71], with pre equilibrium cross-sections by exciton model [72]. Both classical [72] and quantum mechanical [73] approach in pre-equilibrium analysis were introduced and gave better cross section calculations in this code. Reactions with complex particles in the entrance and/or exit channels, mechanisms like stripping, pick-up and knock-out play an important role and these reactions are not covered by the exciton model. Therefore, for the emission of complex particles and complex particle-induced reactions, kalbach's [74] latest systematics are introduced. In total, pre-equilibrium cross section for these reactions is given by the sum of an exciton model, nucleon transfer and knock-out contribution. The default local and global spherical and deformed optical models that are used in this code are quite powerful. All optical model calculations are performed by ECIS-03. The TALYS code uses several level densities, which range from phenomenological analytical expressions to tabulated level densities derived from microscopic models [75]. Energy dependent level density parameter proposed by Ignatyuk et al. [76] is used. The required inputs like nuclear masses, discrete energy levels and level densities of the nuclides involved in the calculations have been taken care in a proper way during the calculations.

4.5.2 Optical model potential

The optical model plays an important role in nuclear reaction calculations. The origin of the optical model potential (OMP) is the interaction between nucleons in the projectile with those in the target nucleus. The aim of the optical model is to find a potential to describe smooth variations of the scattering cross sections as a function of energy and target nucleon number. The main assumption underlying the optical model is that the interaction between an incident particle and a nucleus can be represented by a complex mean field potential, which divides the reaction in to two categories: (i) elastic scattering in which only the direction of the wave propagation is changed and (ii) inelastic scattering in which the particle is scattered into an exit channel different from the incident one. Solving the Schrödinger equation with this complex potential yields among others the reaction and total cross section, the elastic scattering angular distribution, the transmission coefficients that enter the statistical model of compound nucleus

reactions, and the distorted wave functions that are used for the description of direct inelastic scattering to discrete states. In TALYS, all optical model calculations are performed by ECIS-03, which is incorporated as a subroutine.

4.5.3 Pre-equilibrium reactions

It is known that at higher incident energies above about 10 MeV, pre-equilibrium emission contributes significant part of reaction cross section, i.e. it takes place after the first stage of the reaction but long before the compound nucleus attains statistical equilibrium. It is imagined that the incident particle slowly creates more complex states in the compound system and gradually loses its memory how it was formed. Two-component exciton model is used in the TALYS code as a default pre-equilibrium model which has been tested against basically all available experimental nucleon spectra for A > 24.

For pre-equilibrium reactions involving deuterons, tritons, ^{3}He and alpha particles, a contribution from the exciton model is automatically calculated using the default two-component exciton model. It is well known that for nuclear reactions involving projectiles and ejectiles with different particle numbers, mechanisms like stripping, pick-up and knock-out play an important role and these direct reactions are not covered by the exciton model. To deal with this problem, Kalbach [74] developed a phenomenological contribution for these mechanisms, which is included in the TALYS. According to the Kalbach's systematics, the total pre-equilibrium cross section for these reactions is given by the sum of the exciton model (EM), nucleon transfer (NT) and knock-out contribution (KO):

$$\frac{d\sigma_k^{PE}}{dE_k} = \frac{d\sigma_k^{EM}}{dE_k} + \frac{d\sigma_k^{NT}}{dE_k} + \frac{d\sigma_k^{KO}}{dE_k} \tag{4}$$

Where, $$\frac{d\sigma_k^{EM}}{dE_k} = \sigma^{CF} \sum_{p_\pi = p_\pi^0}^{p_\pi^{eq}} \sum_{p_\nu = p_\nu^0}^{p_\nu^{eq}} W_k(p_\pi, h_\pi, p_\nu, h_\nu, E_k) S_{pre}(p_\pi, h_\pi, p_\nu, h_\nu) \tag{5}$$

The details of the Eq. (25) and the description of the terms $\frac{d\sigma_k^{NT}}{dE_k}$ and $\frac{d\sigma_k^{KO}}{dE_k}$ are well explained in ref. [74] and [76] respectively.

4.5.4 Level densities

In TALYS several models for the level densities are introduced, which range from phenomenological analytical expressions to tabulated level densities derived from microscopic models [77]. Gilbert-Cameron model for level density is used as default in this model code. The level density parameter a is energy-dependent and takes into account the damping of shell effects at high excitation energy [76], is given by

$$a(Ex)=\tilde{a}\left[1+\delta W\frac{1-\exp(-\gamma U)}{U}\right] \qquad (6)$$

where, δW is the shell correction energy in MeV which we consider as the difference between the real mass of the nucleus and the mass according to the spherical liquid drop model [77]. The asymptotic level density value $\tilde{a}$ is given by

$$\tilde{a}=\alpha A+\beta A^{2/3} \qquad (7)$$

In which we generally use the parameters

$\alpha = 0.0666, \qquad \beta = 0.2587$

These parameters were obtained from the fit of the Fermi gas level density to all average resonance spacing parameters D_0 of Reference Input Parameter Library (RIPL).

In the present work, we have used neutron energies from 1 keV to 20 MeV for ^{232}Th target. All possible outgoing channels for a given projectile (neutron) energy were considered. However, the cross-sections for the (n,γ) and (n,2n) reactions were specially looked for and collected.

4.6 Result and Discussions

The ^{232}Th(n, γ) reaction cross-section at average neutron energies (E_n) of 3.7±0.3 MeV, 5.9±0.6 MeV, 9.85±0.38 MeV and 15.5±0.7 MeV shown in Table 4.3 are determined for the first time. On the other hand, ^{232}Th(n, 2n) has been re-measured at average E_n of 9.85±0.38 MeV and 15.5±0.7 MeV which are also given in Table. 3. The experimentally determined ^{232}Th(n, γ) and ^{232}Th(n, 2n) reaction cross-sections from the present work have been compared with the evaluated nuclear data from the ENDF/B-VII, JENDL 4.0 and JEFF-3.1. The experimentally measured ^{232}Th(n, γ) and ^{232}Th(n, 2n) reaction cross-sections have been plotted along with the literature data available in IAEA-EXFOR database, evaluated data (e.g. ENDF/B-VII, JENDL-4.0 and JEFF-3.1) and the theoretical values from TALYS 1.2 in Figs.4.14 and 4.15 respectively. It can be seen from the Fig. 15 that the agreement between the present measurement and the evaluated libraries is rather impressive. On the other hand, TALYS 1.2 is not able to reproduce the data between 1 and 8 MeV. Although the slope seems fairly correct, the shift of TALYS 1.2 creates a disagreement larger than factor of 2 at 5.9 MeV and the position of the dip is not very well constrained. The dip in the ^{232}Th(n, γ) reaction cross-section around neutron energy of 7.3 – 8.5 MeV indicates the opening of the (n, 2n) reaction channel beside the (n, nf) reaction. Beyond the neutron energy of 8.0 MeV, the theoretical ^{232}Th(n, γ) reaction cross-section increases up to neutron energy of 14.5 MeV. The experimentally measured ^{232}Th(n, γ) reaction cross-section at E_n = 14.5 MeV [37] is still not understood by theoretical models (e.g. TALYS 1.2) as well as by the evaluations (e.g. ENDF/B-VII.0, JENDL-4.0 and JEFF-3.1). On the other hand, it is clearly seen from the Fig. 4.14 that ^{232}Th(n, γ) reaction cross-section at average E_n = 15.5±0.7 MeV agrees well with the theoretical and evaluated values. This region is of particular interest from the point of view of the giant dipole resonance (GDR) around neutron energy of 12-18 MeV.

It can be seen from Fig. 4.15 that the experimental and theoretical ^{232}Th(n, 2n) reaction cross-section shows a sharp increasing trend from the neutron energy of 6.6 MeV to 8.0 MeV and thereafter remains constant up to 14.5 MeV. Thus, the increasing trend of ^{232}Th(n, γ) reaction cross-section beyond 8 MeV up to 14.5 MeV (Fig.4.14) is due to constant ^{232}Th(n, 2n) reaction cross-section (Fig. 15). Furthermore, it can be seen from Figs. 4.14 and 4.15 that the ^{232}Th(n, γ) reaction cross-section shows a dip, where the ^{232}Th(n, 2n) reaction cross-section

shows a sharp increasing trend. This is most probably due to the sharing of the excitation energy between ^{232}Th(n, γ) and (n, 2n) reaction channels in the neutron energy range below 14 MeV. Above the neutron energy of 14 MeV, ^{232}Th(n, γ) and (n, 2n) reaction cross-sections show a decreasing trend due to opening of (n, 3n) reaction channels.

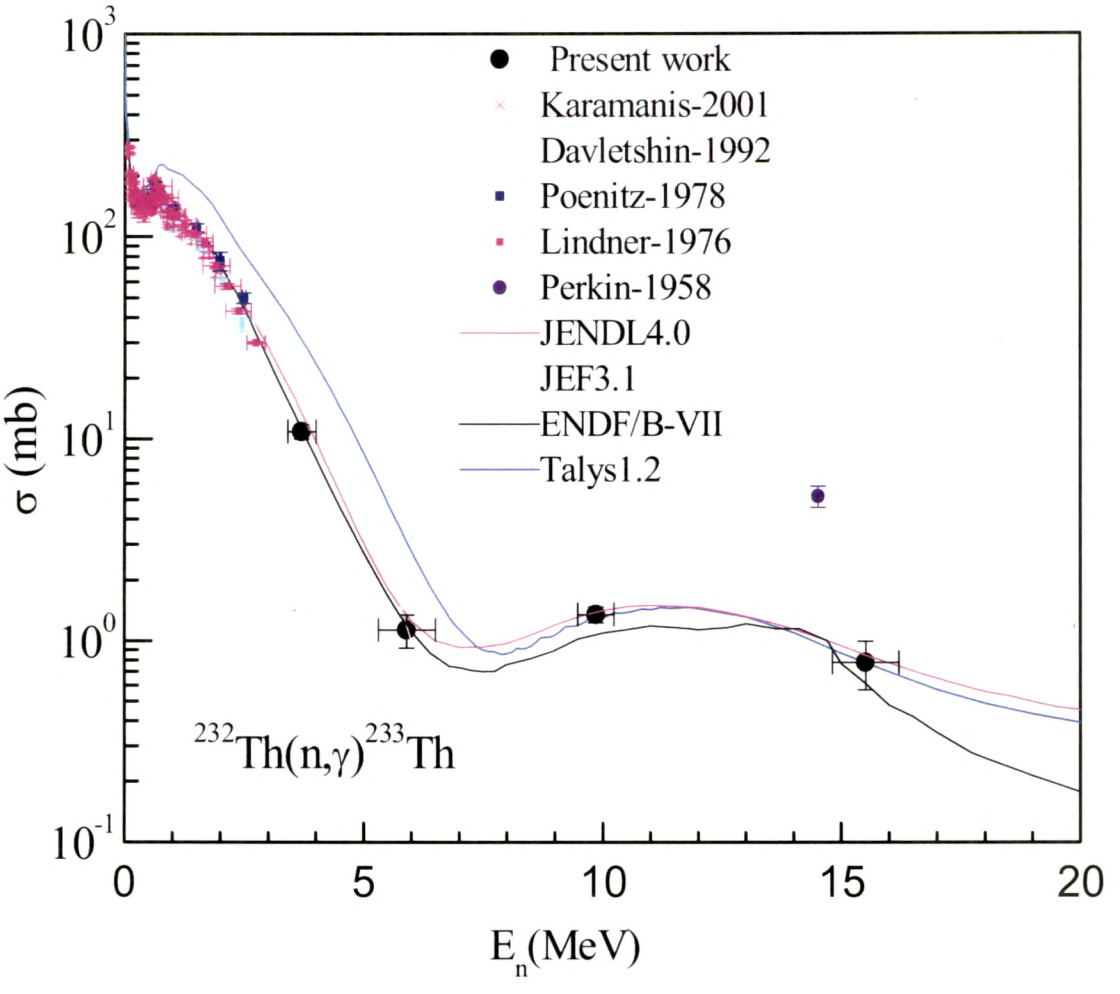

Fig. 4.14 Plot of experimental and evaluated ^{232}Th(n, γ) reaction cross-section as a function of neutron energy from 1 keV to 14 MeV. Experimental values from present work and from ref. [21-37] are in different symbols, whereas the evaluated and theoretical values from TALYS are in solid line of different colors.

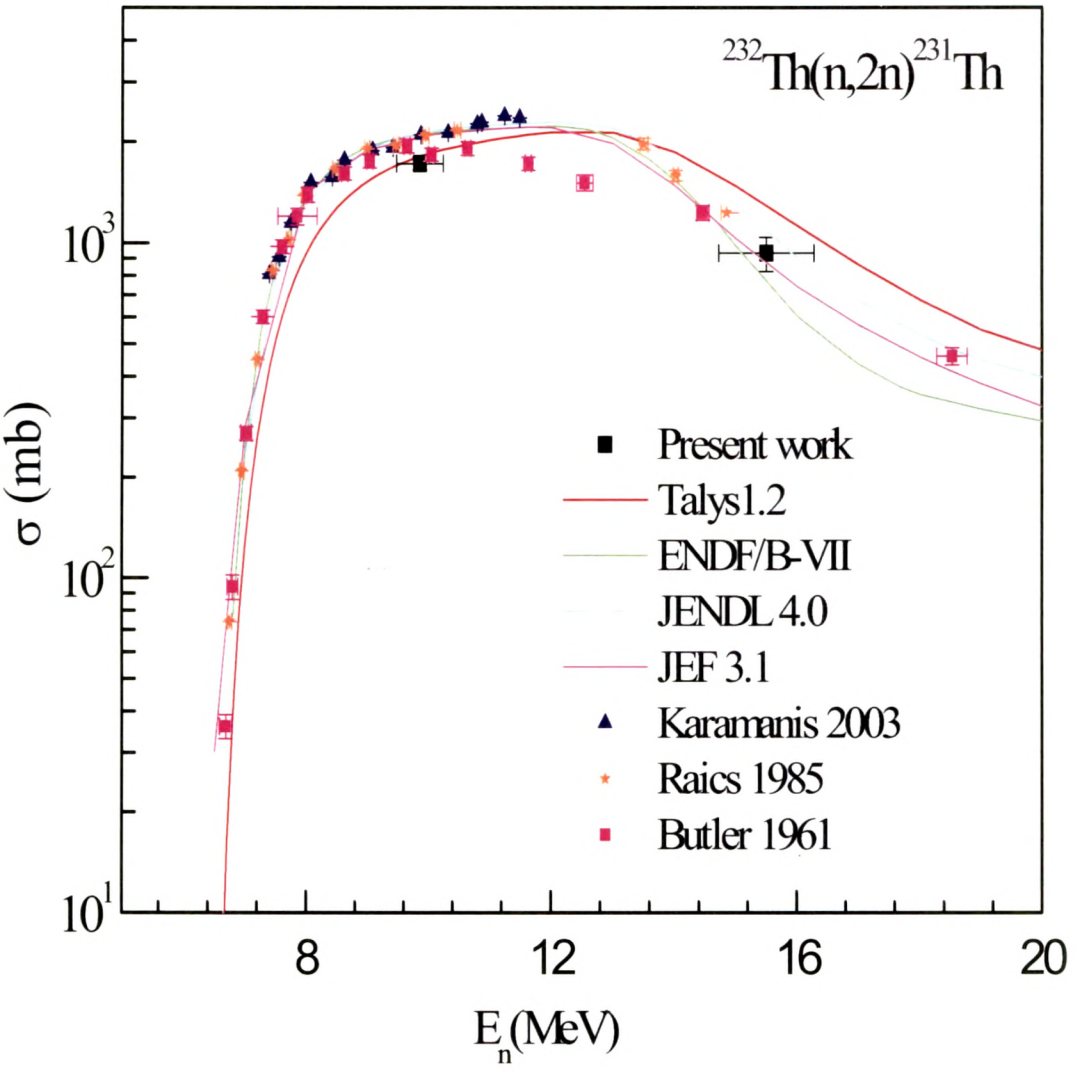

Fig. 4.15 Plot of experimental and evaluated ^{232}Th(n, 2n) reaction cross-section as a function of neutron energy from neutron energy 5 MeV to 20 MeV. Experimental values from present work and from refs. [38-46] are in different symbols, whereas the evaluated and theoretical values from TALYS are in solid lines with different colors.

4.7 Summary and Conclusions

The $^{232}Th(n, \gamma)^{233}Th$ reaction cross-section has been determined using an activation and off-line γ-ray spectrometric technique at average neutron energies of 3.7±0.3 MeV, 5.9±0.6 MeV, 9.85±0.38 MeV and 15.5±0.7 MeV. The $^{232}Th(n, 2n)^{231}Th$ reaction cross-section has also been determined at average neutron energies of 9.85±0.38 MeV and 15.5±0.7 MeV using the same technique. The experiment was carried out using the 14UD BARC-TIFR Pelletron facility at Mumbai, India. The neutron beam was generated using the $^{7}Li(p, n)$ reaction from the proton beam main line at 6 m above the analyzing magnet of the Pelletron facility to utilize the maximum proton current from the accelerator. The experimentally determined cross-sections were compared with latest available evaluated nuclear data libraries of ENDF/B-VII, JENDL 4.0 and JEFF 3.1. The $^{232}Th(n, \gamma)^{233}Th$ and $^{232}Th(n, 2n)^{231}Th$ reaction cross-sections were also calculated theoretically using the nuclear model based computer code TALYS 1.2 and compared with the experimental data. The following conclusions have been drawn from this present work.

a) The $^{232}Th(n, \gamma)$ reaction cross-sections are determined for the first time using the neutron activation technique at average E_n = 3.7±0.3 MeV, 5.9±0.6 MeV, 9.85±0.38 MeV and 15.5±0.7 MeV whereas the $^{232}Th(n, 2n)$ reaction cross-section are a re-measured at average E_n = 9.85±0.38 MeV and 15.5±0.7 MeV using the same technique.

b) The experimental $^{232}Th(n, \gamma)$ reaction cross-sections from present work are in good agreement with the evaluated data from ENDF/B-VII, JENDL-4.0 and JEFF-3.1 at average E_n = 3.7±0.3 MeV, 5.9±0.6 MeV, 9.85±0.38 MeV and 15.5±0.7 MeV. For the $^{232}Th(n, 2n)$ reaction cross-section at average E_n = 9.85±0.38 MeV and 15.5±0.7 MeV, the experimental value lies within the range of the evaluated data.

c) The $^{232}Th(n, \gamma)$ and (n, 2n) reaction cross-sections are calculated theoretically using TALYS 1.2 code and found to be consistent with the experimentally measured data.

d) The experimentally measured $^{232}Th(n, \gamma)$ reaction cross-section at E_n = 14.5 MeV by Perkin at all [37], is now excluded since the measurement at E_n = 15.5 MeV gives more reasonable results.

e) The measurement at E_n = 7 or 8 MeV becomes mandatory in the future to better constrain the model which will have an impact also on evaluations since they are largely based on TALYS calculations.

SMT. HANSA MEHTA LIBRARY
M.S. University of Baroda

References

[1]. F. Carminati et al., "An Energy Amplifier for Cleaner and Inexhaustible Nuclear Energy Production Driven by Particle Beam Accelerator," CERN Report No. CERN/AT/93-47 (ET) (1993)

[2]. C. Rubbia, J. A. Rubio, S. Buono, F. Carminati, N. Fietier, J. Galvez, C. Geles, Y. Kadi, R. Klapisch, P. Mandrilion, J.P. Revol, and Ch. Roche," Conceptual Design of a Fast Neutron Operated High Power Energy Amplifier," CERN/AT/95-44 (ET) 1995.

[3]. American Institute of Physics Conference Proceedings, "The international conference on Accelerator-Driven Transmutation Technologies and Applications, Vol. 346, Las Vegas, Nevada, USA, (1994).

[4]. Accelerator Driven Systems: Energy Generation and Transmutation of nuclear waste, Status report: IAEA- TECDOC- 985 (Nov. 1997).

[5]. C. D. Bowman, "Accelerator-Driven Systems for Nuclear Waste Transmutation," Ann. Rev. Nucl. Part. Sci, **48**, 505 (1998)

[6]. S. Ganesan, Pramana J. Phys., **68**, 257 (2007).

[7]. R.K. Sinha and A. Kakodkar, "Design and Development of AHWR – The Indian Thorium Fueled Innovative reactor," Nucl. Eng. Des. **236**, 7-8, 683 (2006)

[8]. S. Ganesan, "Creation of Indian Experimental Benchmarks for Thorium Fuel Cycle," IAEA Coordinated research project on "Evaluated Data for Thorium- Uranium fuel Cycle," Third Research Co-ordination Meeting, 30 January to 2 February 2006, Vienna, Austria, INDC (NDS) - 0494 (2006).

[9]. L. Mathieu et al., "Proportion for a very simple Thorium Molten Salt reactor," Proc. Global International Conference, Paper No. 428, Tsukuba, Japan, 2005

[10]. Fast Reactors and Accelerator Driven Systems Knowledge Base, IAEA-TECDOC-1319: Thorium fuel utilization: Options and Trends

[11]. A. Nuttin et al., Proc. Nucl. Energy **46**, 77 (2005)

[12]. T.R. Allen and D.C. Crawford, Science and Technology of Nuclear Installations, Article ID 97486 (2007).

[13]. V. G. Pronyaev, "Summary Report of the Consultants' Meeting on Assessment of

Nuclear Data Needs for Thorium and Other Advanced Cycles," INDC (NDS) - 408, International Atomic Energy Agency (1999)

[14]. B. D. Kuz'minov and V. N. Manokhin, "Status of Nuclear Data for Thorium Fuel Cycle," Nucl. Constants, Issue No.3-4, **41** (1997)

[15]. E. T. Cheng and D. R. Mathews, "The Influence of Nuclear Data Uncertainties on Thorium Fusion-Fission Hybrid Blanket Nucleonic Performance," Proc. Int. Conf. Nuclear Cross Sections for Technology, Knoxville, Tennessee, October 22-26, 1979, p. 834, NBS-SP 594, National Bureau of Standards

[16]. D. E. Bartine, "The Use of Thorium in Fast Breeder Reactors," Proc. Int. Conf. Nuclear Cross Sections for Technology, Knoxville, Tennessee, October 22-26, 1979, p. 119, NBS-SP 594, National Bureau of Standards

[17]. S. Pelloni, G. Youinou and P. Wydler, "Impact of Different Nuclear data on the Performance of fast spectrum based on the Thorium-Uranium fuel cycle," Proc. Int. Conf. Nuclear data for Science and Technology, Trieste, Italy, May 19-24, 1997, part II, p.1172

[18]. M. Salvatores, "Experimental Facilities, Training and Expertise in the Nuclear Data Field: Needs and gaps for reactor physics applications," Nuclear Data for Science and Technology (Proc. Int. Con. Trieste, 1997), Vol. 59, part I (G. Reffo, A. Ventura, and C. Grandi, Eds.), Italian Physical Society, Bologna (1997) 3-17.

[19]. S. S. Kapoor, Pramana J. Phys. **59**, 941 (2002)

[20]. IAEA-EXFOR Database, at http://www-nds.iaea.org/exfor

[21]. R. C. Little, R. C. Block, D. R. Harris, R. E. Slovacek and O. N. Carlson, Nucl. Sci. Eng., **79**, 175 (1981)

[22]. A. Borella et al., Nucl. Sci. Eng., **152**, 1 (2006)

[23]. G. Aerts et al., Phys. Rev. C **73**, 054610 (2006)

[24]. H. Pomerance, Phys. Rev. **88**, 412 (1952)

[25]. R. L. Macklin, N. H. Lazar and W. S. Lyon, Phys. Rev. **107**, 504 (1957)

[26]. J.A. Miskel, K.V. Marsh, M. Lindner and R.J. Nagle, Phys. Rev. **128**, 2717 (1962)

[27]. D. C. Stupegia, B. Smith and K. Hamm, J. Inorg. Nucl. Chem. **25**, 627 (1963)

[28]. M. C. Muxon, TRDWP/P-8, U.K. Atomic Energy Authority, Harwell (1963)

[29]. L. Forman, A.D. Schelberg, J.H. Warren and N.W. Glass, Phys. Rev. Lett. **27**, 117 (1971)

[30]. V.B. Chelnokov et al. USSR Obninsk Report Jaderno Fizicheskii Issledovanija-13 P. 16 (Oct. 1972).

[31]. M. Lindner, R. J. Nagle and J. H. Landrum, Nucl. Sci. Eng. **59**, 381 (1976)

[32]. R. E. Chrien, H. I. Liou, M. J. Kenny and M. L. Stelts, Nucl. Sci. Eng. **72**, 202 (1979)

[33]. G.T. Baldwin and G.F. Knoll, Nucl. Sci. Eng. **88**, 123 (1984)

[34]. R. T. Jones, J. S. Merritt and A. Okazaki, Nucl. Sci. Eng. **93**, 171 (1986)

[35]. K. Wisshak, F. Voss and F. Kappeler, Nucl. Sci. Eng. **137**, 183 (2001)

[36]. D. Karamanis et al., Nucl. Sci. Eng. **139,** 282 (2001)

[37]. J. L. Perkin, L. P. O'connor, R. F. Colemann, Proc. Phys. Soc. (London), **72**, 505 (1958)

[38]. R. J. Prestwood and B.P. Bayhurst, Phys. Rev. **121**, 1438 (1961)

[39]. J.P. Butler and D. C. Santry, Can J. Chem., **39**, 689 (1961)

[40]. R. Batchelor, W. B. Gilboy, J. H. Towle, Nucl. Phys. **65**, 236 (1965)

[41]. M. Bormann, Nucl. Phys. **65**, 257 (1965)

[42]. H. Karius, A. Ackermann and W. Scobel, J. Phys (G) **5**, 715 (1979)

[43]. H. Chatani, Nucl. Inst. Methods. **205**, 501 (1983)

[44]. P. Raics, S. Daroczy, J. Csikai, N.V. Kornilov, V. Ya. Baryba and O.A. Salnikov, Phys. Rev. C **32**, 87 (1985)

[45]. D. Karamanis et al., Nucl. Instrum. Methods Phys. Res. A, **505**, 381 (2003)

[46]. J. Adam et al., Eur. Phys. J. A. **23**, 61 (2005).

[47]. M.B. Chadwick et al., Nucl. Data Sheets, **107**, 2931 (2006)

[48]. K. Shibata et al., J. Nucl. Sci. Technol., **48**, 1, (2011).

[49]. A. J. Koning et al., The JEFF evaluated data project, in Proceeding of the International Conference on Nuclear Data for Science and Technology, Nice, 2007 (EDP Sciences, 2008)

[50]. A.J. Koning, S. Hilaire, M.C. Duijvestijn, Proceeding of the International Conference on Nuclear Data for Science and Technology, ND 2004, Santa Fe, 2004, Edited by R.C.

Haight, M. B. Chadwick, T. Kawano, P. Talou, AIP Conf. Proc. **769**, 1154 (2005)

[51]. S. G. Mashnik et al., ^{7}Li(p,n) Nuclear data Library for Incident Proton Energies to 150 MeV, arXiv: nucl-th/00110666v117, Los Alamos National Laboratory (Nov.2000)

[52]. S. S. Kapoor "BARC News Letter" No. 91, June 1991

[53]. S. C. Sharma, et al., "Commissioning of Proton Beam Irradiation Setup at BARC-TIFR Pelletron Accelerator Facility, Mumbai" DAE-BRNS Symposium on Nuclear Physics-2003

[54]. J. F. Ziegler, M. D. Zeigler, J. P. Biersack, Nucl. Inst. Meth. B, 268, 1818 (2010)

[55]. J. W. Meadows, D. L. Smith, Neutrons from proton bombardment of natural Lithium, Argone National Laboratory Report ANL-7983 (1972).

[56]. NuDat (BNL, U.S. A), www.nndc.bnl.gov/nudat2/

[57]. R. R. Borchers, C. H. Poppe, Phys. Rev. **129**, 2679 (1963)

[58]. H. Liskien and A. Paulsen, "Neutron Production Cross Sections and Energies for the Reactions ^{7}Li(p,n)^{7}Be and ^{7}Li(p,n)^{7}Be*," At. Data Nucl. Data Tables, 15, 57 (1975)

[59]. M. Herman, "Statistical Model Code Empire-II", available on the Internet at http://www-nndc.bnl.gov/empire 2.19/

[60]. C. H. Poppe, J. D. Anderson, J.C. Davis, S.M. Grimes, and C. Wong, Phys. Rev. C **14**, 438 (1976)

[61]. P. K. Mukhopadhyaya, Personal Communication (2001)

[62]. "The international Reactor Dosimetry File:IRDF-2002", Nuclear Data Section, International Atomic Energy Agency

[63]. J. Blachot, Nuclear Data Sheets, **104**, 967-1110 (2005)

[64]. L. E. Glendenin et al., Phys. Rev. C **22**, 152 (1980)

[65]. J. Blons, C. Mazur, and D. Paya, Phys. Rev. Lett. **35**, 1749 (1975)

[66]. Sun Tungyu, Li Wenxin, Dong Tianrong, Fu ming, J. PHE. **12**, Issue no.2, 221(1988)

[67]. B. Singh, J. K. Tuli, Nuclear Data Sheets **105**, 109-222 (2005)

[68]. E. Browne, Nuclear Data Sheets **93**, 763 (2001); E. Browne and R.B. Firestone, Table of Radioactive Isotopes, ed. V.S. Shirley (1986)

[69]. J. Raynal, Notes on ECIS94, CEA Saclay Report No. CEA-N-2772, (1994).

[70]. A. J. Koning and J. P. Delaroche, Nucl. Phys. A **713**, 231 (2003)

[71]. Hauser, W., Feshbach, H., Phys. Rev. **87**, 366 (1952)

[72]. A. J. Koning and M. C. Duijvestijn, Nucl. Phys. A **744,** 15 (2004)

[73].H. Gruppelaar, P. Nagel and P. E. Hodgson, Riv. Nuovo Cimento 9, No. 7, 1 (1986)

[74]. C. Kalbach, Phys. Rev. C **71**, 034606 (2005)

[75]. A. J. Koning, S. Hilaire and S. Goriely, Nucl. Phys.A, **810**, 13 (2008)

[76]. A. V. Ignatyuk, G. N. Smirenkin and A. S. Tishin, Sov. J. Nucl. Phys. **21**, no. 3, 225 (1975)

[77]. W. D. Myers and W. J. Swaiatecki, Nucl. Phys. **81**, 1 (1966)